ELSEVIER

Biophysical Chemistry 50 (1994) 255–271

Biophysical Chemistry

Electrostatic effects in short superhelical DNA ☆

Marcia O. Fenley, Wilma K. Olson *, Irwin Tobias, Gerald S. Manning

Department of Chemistry, Rutgers, the State University of New Jersey, New Brunswick, NJ 08903, USA

(Received 28 April 1993; accepted 1 November 1993)

Abstract

We present Monte Carlo simulations of the equilibrium configurations of short closed circular DNA that obeys a combined elastic, hard-sphere, and electrostatic energy potential. We employ a B-spline representation to model chain configuration and simulate the effects of salt on chain folding by varying the Debye screening parameter. We obtain global equilibrium configurations of closed circular DNA, with several imposed linking number differences, at two salt concentrations (specifically at the extremes of no added salt and the high salt regime), and for different chain lengths. Minimization of the composite elastic/long-range potential energy under the constraints of ring closure and fixed chain length is found to produce structures that are consistent with the configurations of short supercoiled DNA observed experimentally. The structures generated under the constraints of an electrostatic potential are less compact than those subjected only to an elastic term and a hard-sphere constraint. For a fixed linking number difference greater than a critical value, the interwound structures obtained under the condition of high salt are more compact than those obtained under the condition of no added salt. In the case of no added salt, the electrostatic energy plays a dominant role over the elastic energy in dictating the shape of the closed circular DNA. The DNA supercoil opens up with increasing chain length at low salt concentration. A branched three-leaf rose structure with a fixed linking number difference is higher in energy than the interwound form at both salt concentrations employed here.

Key words: Superhelical DNA; Electrostatics; Monte Carlo simulations; Simulated annealing

1. Introduction

The perfect linear structure of the Watson–Crick B-DNA helix is distorted in compactly folded, naturally occurring DNA. The common axis of the double helix winds in space to form a new helix of a higher order, termed a supercoil or superhelix. While many viral DNAs adopt branched and interwound covalently closed supercoiled forms [1], the DNA in chromatin (a complex of the double helix with protein) of higher organisms wraps around a core of protein to form a left-handed solenoidal superhelix. Supercoiling can thus be manifested by any spatially constrained sequence (including short linear chains), and also can be expressed in both a

* Corresponding author.

☆ Taken in part from the dissertation submitted by Marcia O. Fenley in fulfillment of the requirements for the degree of Doctor of Philosophy, Rutgers, the State University of New Jersey (1991).

SSDI 0301-4622(93)E0094-L

negative and a positive sense [1,2]. In living organisms there is roughly one superhelical turn for every twenty turns of the local helix (e.g., ≈ 200 base pairs (bp)) [1,3]. Not surprisingly, DNA supercoiling is an important facet of biological processes that entail local helical winding and unwinding, such as replication, transcription, and recombination. The closed circularity and the deformations associated with supercoiling affect many physical and chemical properties of the double helix, including its hydrodynamic behavior, energetics, and enzymology.

The spatial constraints of DNA supercoiling can be characterized mathematically by White's formula [4],

$$Lk = Tw + Wr. \quad (1)$$

Here Lk is the linking number of DNA or the number of times the two strands of the duplex are intertwined (total number of revolutions of one strand about the other), Tw is the twist of one strand around the double-helical axis (expressed as helical turns), and Wr is the writhing number, a measure of certain aspects of the tertiary folding of the helix axis in space. From Eq. (1), it follows that $\Delta Lk = \Delta Tw + Wr$, where $\Delta Tw = Tw - Tw_0$ and Tw_0 is the twist in the torsionally relaxed ($Tw = Tw_0$) state.

Until now, theoretical studies of supercoiled DNA have been based on an elastic model, where the DNA is described as an uncharged, isotropic, symmetric, and linearly elastic thin rod characterized by its bending and twisting stiffness. The forces opposing the deformation of the rod give rise to two independent energy contributions, one which corresponds to the local bending of the double helical axis and one which corresponds to the twisting of the duplex with respect to its equilibrium rest state. The two contributions are expressed, respectively, in terms of the integral of the square of the curvature and the square of the total twist (see the following section). It is important to relax the simplifying assumption of DNA as an uncharged rod given the charged phosphate groups along its chemical backbone. It is expected for a charged macromolecule, such as DNA, that the shape of its supercoiled structures should be strongly dependent on ionic environment; that is, electrostatic effects should play a significant role in dictating the long-range folding of the polymer. In this paper, we treat supercoiled DNA more realistically than ever before by taking into account the polyelectrolyte character of the chain backbone. To our knowledge, this is the first computer simulation of supercoiled DNA to treat electrostatic effects explicitly. In the past, ionic effects in supercoiled DNA have been treated only approximately in terms of variable hard-sphere contact limits (see, for example, Ref. [5]).

We consider the polyelectrolyte and elastic behavior of DNA as well as excluded volume effects (i.e. the interactions that arise because the chain segments occupy a finite volume and thus cannot self-intersect) in computer simulations of the minimum energy superhelical configurations. As in previous studies [5–7], we employ a B-spline representation to model the spatial trajectory of closed circular DNA and carry out Monte Carlo/simulated annealing calculations. In order to examine the role of the polyelectrolyte backbone on the folding of the chain, we adopt a more physical potential which, besides elastic and hard-sphere contributions, includes a modified Debye–Hückel energy contribution. By varying the Debye screening parameter we can simulate the effects of salt on chain folding. As a first step, we study short chains of 100–175 bp, which can be treated rigorously within the context of the modified Debye–Hückel potential. We obtain minimum energy configurations of closed circular DNA with several imposed linking number differences, ΔLk, at two salt concentrations (specifically at the extremes of no added salt and the high salt region), and at different chain lengths. This study allows us to examine how the variation of salt concentration affects the superhelical configurations of DNA. We compare our results with corresponding computer simulations of closed circular DNA [6,7] based on the simple elastic model (with excluded volume effects) and further discuss our findings in the context of the observed changes in overall shape of comparable short DNAs in cryo-electron microscopic images at low and high salt concentration [8,9].

2. Model and method

The isotropic elastic rod model has been used for many years to model closed circular DNA [10–16]. Only recently have the excluded volume effects, which are important to long interwound DNAs, been taken into account [5–7,17–19]. As noted above, superhelical DNA is treated even more physically in this paper by directly taking into consideration the polyelectrolyte character of DNA.

2.1. B-spline representation

The axis of the closed double-helical trajectory is represented by piecewise cyclic B-spline curves [20]. The B-splines are defined by a series of polynomial expressions which smoothly connect a given sequence of controlling points (14 for the circle and interwound forms and 15 for the branched three-leaf rose configuration modeled here). These curves are regionally defined functions that are evaluated separately over different intervals of the chain trajectory with as many continuous derivatives as needed for the mathematical analyses to be performed. Since only continuous first and second derivatives are required for the calculation of the differential geometric (e.g., writhing number and curvature integral) and the energetic parameters of the elastic DNA model, we employ order 4 (cubic) B-splines. Furthermore, the cyclic form of the curves automatically satisfies the ring closure constraints of closed circular or looped DNA and provides descriptions of arbitrary trajectories of the double-helical axis for which there are not necessarily explicit geometric expressions. The configuration of the chain is modified by simply varying the coordinates of the controlling points. For a more detailed discussion of the B-spline methodology, the reader is referred elsewhere [5–7,18]. Chains of different contour lengths (100–175 bp) are obtained by rescaling the controlling points of the initial chain configuration. The phosphate groups, which are represented by individual phosphorus atoms, are evenly spaced at ≈ 1.7 Å increments of arc length along the double-helical axis (represented by the B-spline curve). This spacing is consistent with the projection of phosphate groups of complementary-strands on the helical axis of the canonical B-DNA duplex [21].

2.2. Potential energy

We assume that the total energy E of the closed circular DNA has four terms. The first two terms, a bending E_B and a twisting E_T contribution, take into account the elastic character of a homogeneous isotropic thin rod. The third contribution E_{HS} monitors excluded volume effects by means of a hard-sphere potential. The last contribution E_{EL} treats the polyelectrolyte character of DNA. The charges on the phosphate groups, which are reduced in magnitude to account for the counterion condensation phenomenon [22], interact via a modified Debye–Hückel potential. Therefore, the total energy is expressed as

$$E = E_B + E_T + E_{HS} + E_{EL}. \tag{2}$$

The bending energy E_B of the superhelical DNA is given by

$$E_B = \frac{A}{2}\int_0^L \kappa(s)^2 \, ds, \tag{3}$$

where κ is the curvature of the axis of the rod, s the arc length, L the total contour length of the DNA (prior to scaling), and A the bending stiffness constant. The magnitude of A is determined from the per residue step height h of DNA (3.4 Å), the per residue mean-square bending angle $\langle \Lambda^2 \rangle$ (in units of radians), the Boltzmann constant k, and the absolute temperature T using the expression $A = 2hkT/\langle \Lambda^2 \rangle$ [23]. The persistence length P_t is also related to A through the relation $P_t = A/kT$ [24]. Taking the root-mean-square bending angle to be 8.5° at 298 K yields $A = 1.2755 \times 10^{-11}$ erg Å and $P_t = 310$ Å. The latter value corresponds roughly to the non-electrostatic contribution to the persistence length of DNA in aqueous NaCl solution [25].

The twisting energy E_T of the superhelical DNA is expressed as

$$E_T = \frac{C}{2}\int_0^L (\omega - \omega_0)^2 \, ds, \tag{4}$$

where ω is the rate of local twist per unit arc length (i.e. twist density), ω_0 the intrinsic rate of twist, and C the twisting stiffness constant. The expression $C = hkT/\langle\phi^2\rangle$ [26,27] is used to compute the force constant. The parameter $\langle\phi^2\rangle$ in this equation is the mean-square twisting angle in units of radians. Assuming a bending/twisting stiffness ratio $A/C = 1$ and setting h, k, and T to the values listed above gives $C = 1.2755 \times 10^{-11}$ erg Å (since $A = 1.2755 \times 10^{-11}$ erg Å) and a root-mean-square twisting angle $\langle\phi^2\rangle = 6°$. The case $A/C = 2$ is also considered, the chosen ratio corresponding to $A = 2.5510 \times 10^{-11}$ erg Å and $\langle\lambda^2\rangle = 6.0°$.

According to Fuller [13] and Tanaka and Takahashi [28], if the rod is isotropic, symmetric, and linearly elastic and the twist density is consequently uniform, the expression for E_T given in Eq. (4) can be rewritten as

$$E_T = \frac{2\pi^2 C}{L}(\Delta Lk - Wr)^2. \tag{5}$$

This simplification follows from the integral in Eq. (4), which under these conditions can be rewritten as $(\omega - \omega_0)^2 L$, together with the identity $(\omega - \omega_0)L = 2\pi\Delta Tw$ and White's formula, $\Delta Tw = \Delta Lk - Wr$. Here ΔLk is the imposed linking number difference of superhelical DNA relative to the relaxed (unwrithed) closed circular form and Wr is the writhing number. Local secondary structural effects, such as salt induced changes in intrinsic helical twist or major conformational transitions (e.g., B- to A-DNA or right- to left-handed transitions), are thus ignored in the calculations. We calculate the writhing number using either the Gauss double integral [29] or Fuller's single integral [30]. For a detailed presentation of these equations, the reader is referred elsewhere [6,7]. Eqs. (3)–(5) follow from the assumptions that the rod is intrinsically straight, has a circular cross-section, and therefore exhibits no preferential directions of bending and twisting.

A hard-sphere potential E_{HS} is used to account for long-range excluded volume effects. This energy contribution prevents the self-intersection of chain segments that are far apart along the DNA contour. The contacts of chain contour points are thus restricted to distances greater than a cutoff radius D with E_{HS} given by

$$E_{HS} = \begin{cases} \infty & r_{jk} \leqslant D, \\ 0 & r_{jk} > D. \end{cases} \tag{6}$$

The parameter r_{jk} is the distance between any two points along the double-helix axis. In practice, only values j and k separated by an arc length greater than ≈ 68 Å (roughly two helical turns of the DNA duplex) are considered, and the parameter D is set equal to the diameter of DNA (≈ 20 Å).

The modified Debye–Hückel energy E_{EL} between any phosphate pair along the double-helical axis is given by:

$$E_{EL} = (q')^2 \sum_{j<k}^{P} \frac{e^{-\kappa r_{kj}}}{\epsilon r_{jk}}. \tag{7}$$

Here P is the total number of phosphate groups, r_{jk} the distance between the jth and kth phosphate groups, ϵ the dielectric constant of water at 25° (i.e. 78.3), and q' the effective phosphate charge (i.e. the phosphate charge reduced by $1 - N\theta_N$ to account for the counterion condensation phenomenon, with θ_N the number of condensed N-valent counterions per DNA charge). According to counterion condensation theory for B-DNA in an environment of aqueous NaCl solution [22], there is 76% neutralization of the phosphate charges by bound Na^+ ions. It follows that $1 - N\theta_N = 0.24$ and the effective charge q' is given by $q \times 0.24$, where q is the unit electrical charge. The parameter κ in Eq. (7) (not to be confused with the curvature introduced above) is the Debye screening parameter given by,

$$\kappa = 0.329\sqrt{c_s}, \tag{8}$$

with c_s the concentration of monovalent salt in units of molarity. Two extreme cases are considered: no added salt ($c_s = 0$ M) and the high salt regime ($c_s = 1$ M). The usual mixing and entropic contributions to the ionic free energy within the framework of numerical counterion condensation theory are neglected in the current studies.

In some supercoiled configurations two DNA segments can approach closely enough to pene-

trate each other's Debye clouds. Therefore, the effective charges (q' in Eq. (7)), which we take as invariant according to the counterion condensation theory of a single isolated polyion, become more approximate when two segments are close. This approximation, however, is unlikely to lead to qualitatively incorrect results. Furthermore, even with this difficulty, the Debye–Hückel potential with invariant effective charges is better than a Debye–Hückel potential with bare charges (valence = −1); the condensed counterions lower the charge on the phosphates by at least some amount, even if this amount changes as segments approach one another.

The total energy is expressed in reduced form as $\tilde{E}$, a dimensionless quantity obtained by dividing the total energy in Eq. (2) by the constant $2\pi^2 C/L$.

The superhelical configurations described below are also subject to a contour length constraint not included in the total energy. The chain length is preserved by using the following harmonic expression:

$$E_L = K_L(L - L_0)^2. \tag{9}$$

Here K_L is a stretching force constant, taken as 0.3 erg Å^{-2}, L_0 the initial contour length, and L the actual contour length. This pseudo-potential allows the chain to fluctuate to a small degree during the course of the simulation. If the contour length is kept strictly constant, few moves can be made, even at high temperatures.

2.3. Monte Carlo simulation

In order to identify the global minimum of the total energy (in reduced energy units) under the constraints of ring closure and chain length, we use an algorithm that combines Metropolis Monte Carlo sampling [31] with a simulated annealing procedure [32]. The starting configuration is either a circle (in most cases) or a branched three-leaf rose structure. The B-spline controlling points are moved at random with new configurations of lower energy automatically accepted and those of higher energy accepted on the basis of the Boltzmann factor of the increase in energy. The system is allowed to approach an equilibrium distribution at a given starting temperature T_0. The starting temperature T_0 is obtained from the expression $kT_0 = \sigma E_0$, where k is the Boltzmann constant, E_0 the starting initial energy, and σ set equal to 0.01. This value of σ guarantees that 30%–50% of the moves among all trials are accepted. The temperature is then reduced by an accelerated cooling procedure where the temperature is lowered by a factor 0.95^p at the pth temperature lowering step, and the system is allowed to reach equilibrium once again. At each temperature, the configuration is relaxed by 20000 Monte Carlo moves. The step size is set equal to 0.8% of the initial contour length of the DNA. The cooling process is allowed to take place 17 times, but is terminated early if the configuration no longer changes (i.e. when the temperature is below the freezing point).

3. Results and discussion

We have employed the method outlined in the previous section to examine the optimized superhelical configurations of DNA subject to the composite elastic/electrostatic potential energy. We obtain minimum energy superhelical configurations of DNA, with several imposed linking number differences, at different salt concentrations and chain lengths. We have also compared the features of the elastic/electrostatic model with those of previously reported elastic models of superhelical DNA.

3.1. Dependence of supercoiled configuration on linking number difference and salt concentration

We begin by examining the dependence of the superhelical configurations of a 100 bp DNA on the linking number difference under the constraints of ring closure and controlled chain length. To study the ionic strength dependence of the onset of supercoiling, we have started with a perfect circle and varied ΔLk from 0 to 4 under two extreme salt conditions. We fix A/C equal to unity and consider the cases of no added monovalent salt (i.e. NaCl) ($c_s = 0$ M) and the

high salt regime ($c_s = 1$ M). We anticipate that the repulsion between phosphate groups will delay the onset of supercoiled states, in which the average distance between phosphate groups is reduced compared to the open circle. We further expect that this repulsion will be greater in the absence of salt since the phosphate groups are unscreened by small ions.

In order to gain a better idea about the overall shape of the optimized DNA structures we compute the radius of gyration (R_g), the principal moments of the radius of gyration (I_1, I_2, I_3, where $R_g^2 = I_1^2 + I_2^2 + I_3^2$), and the average interphosphate distance ($\langle P \ldots P_{dist} \rangle$) of the resulting DNA structures. For a discussion of the procedure employed to compute the principal moments of the radius of gyration, the reader is referred elsewhere [18].

The final optimized configurations obtained for integral values of the imposed linking number difference under the condition of no added salt are illustrated in Fig. 1a. These and selected intermediate states are described in further detail in Tables 1 and 2. As evident from the reported data, the minimum energy configurations of the DNA are circles for values of ΔLk up to at least 2.5. The radii of gyration, principal moments of gyration, average interphosphate distances, and writhing number are roughly the same for the optimized structures over this range. Moreover,

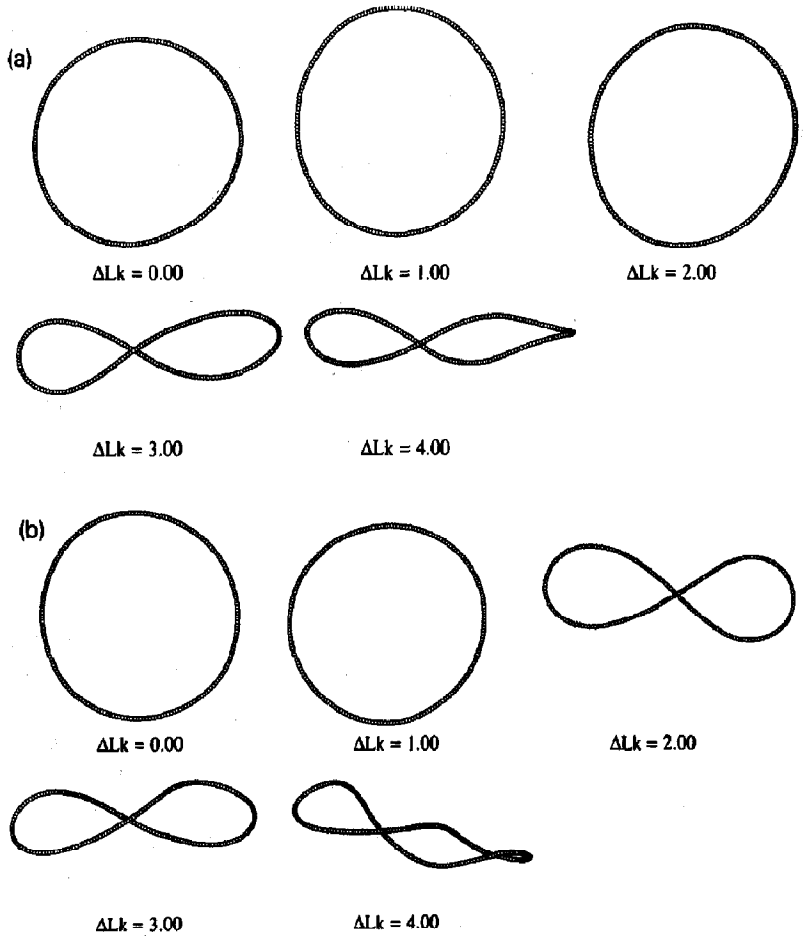

Fig. 1. Optimized supercoiled configurations of 100-residue DNA supercoils (200 phosphates) at various imposed linking number differences for (a) $c_s = 0$ M (no added salt) and (b) $c_s = 1$ M salt concentrations. Electrostatic interactions are represented by a modified Debye–Hückel potential and excluded volume effects by a hard-sphere potential. The starting configuration is a circle of 14 evenly spaced controlling points.

Table 1
Radius of gyration (R_g), principal moments of the radius of gyration (I_1, I_2, I_3) and the average P...P distance $\langle P...P_{dist} \rangle$ as a function of ΔLk and salt concentration [a]

ΔLk	R_g (Å)	I_1 (Å)	I_2 (Å)	I_3 (Å)	$\langle P...P_{dist} \rangle$ (Å)
$c_s = 0$ M					
0.00	53.71	38.39	37.53	1.59	69.14
1.00	53.74	38.21	37.78	1.11	69.18
2.00	53.69	39.36	36.48	1.31	69.09
2.50	53.76	38.45	37.57	0.71	69.20
2.75	44.76	41.95	14.47	5.84	55.44
3.00	44.89	42.51	13.33	5.45	55.30
4.00	44.29	42.73	9.34	7.00	53.89
$c_s = 1$ M					
0.00	53.76	38.50	37.50	0.98	69.20
1.00	53.77	38.41	37.63	0.62	69.21
1.50	53.71	38.63	37.29	1.56	69.14
1.75	44.48	41.29	15.16	6.62	55.34
2.00	44.64	41.91	14.38	5.44	55.24
3.00	43.89	41.98	10.72	6.99	53.75
4.00	43.44	41.86	9.08	7.19	52.86

[a] The elastic and electrostatic model was used with $A/C = 1$ and 100 bp chain length.

Table 2
Writhing number and reduced energy components as a function of ΔLk and salt concentration [a]

ΔLk	Wr	$\tilde{E}$	$\tilde{E}_B$	$\tilde{E}_T$	$\tilde{E}_{EL}$
$c_s = 0$ M					
0.00	0.00	15.64	1.01	0.00	14.63
1.00	0.00	16.63	1.00	1.00	14.63
2.00	0.01	19.63	1.02	3.97	14.64
2.50	0.06	21.61	1.03	5.95	14.63
2.75	0.86	22.96	2.88	3.58	16.50
3.00	0.96	23.98	3.20	4.15	16.63
4.00	1.39	28.74	4.69	6.83	17.22
$c_s = 1$ M					
0.00	0.00	3.28	0.99	0.00	2.29
1.00	0.04	4.23	1.02	0.92	2.29
1.50	0.00	5.56	1.03	2.24	2.29
1.75	0.80	5.96	2.77	0.90	2.29
2.00	0.93	6.51	3.07	1.15	2.29
3.00	1.22	9.55	4.07	3.19	2.29
4.00	1.60	13.17	5.13	5.75	2.29

[a] The elastic and electrostatic model was used with $A/C = 1$ and 100 bp chain length. The energy, $\tilde{E} = E/(2\pi^2 C/L)$, is a non-dimensional quantity.

the shapes are very close to those of a perfect circle, for which $R_g = (100 \text{ bp} \times 3.4 \text{ Å/bp})/2\pi = 54.11$ Å, $I_1 = I_2 = R_g/\sqrt{2} = 38.26$ Å, and $I_3 = 0$. The supercoiled forms found to be of low energy at $\Delta Lk = 2.75$ and beyond, however, are quite different in overall shape from the circle. The relative compactness of these structures is immediately apparent from the decreased values of both the radii of gyration and the average interphosphate distances in Table 1 as well as from

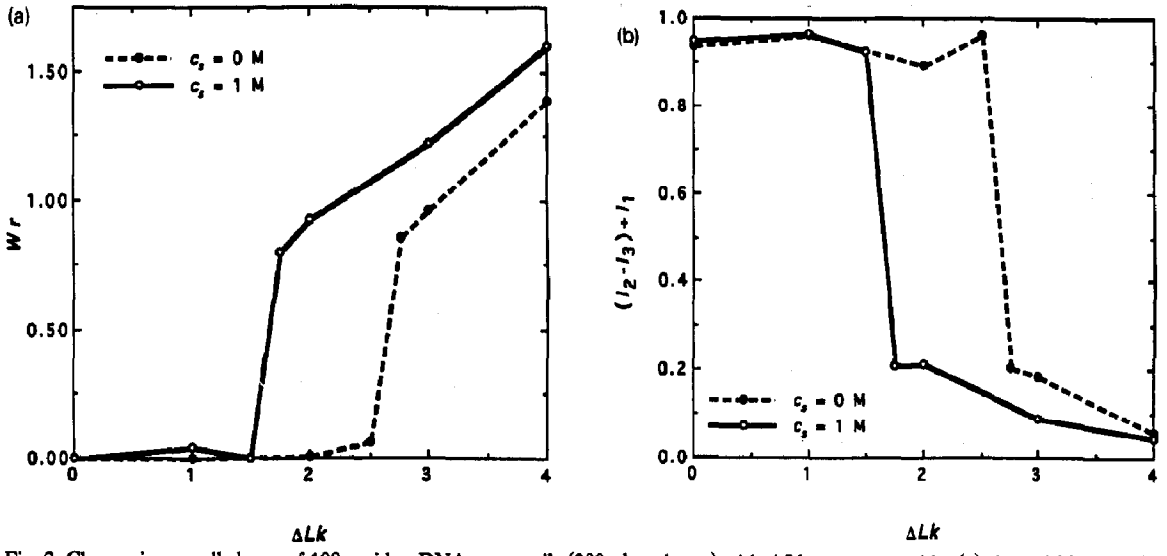

Fig. 2. Change in overall shape of 100-residue DNA supercoils (200 phosphates) with ΔLk as measured by (a) the writhing number Wr and (b) the ratio $(I_2 - I_3)/I_1$ of principal moments of the radius of gyration, at $c_s = 0$ M (no added salt) and $c_s = 1$ M. The elastic and electrostatic model was used with $A/C = 1$ and 100 bp chain length. See legend to Fig. 1.

the molecular representations in Fig. 1a. The magnitudes and relative proportions of the principal moments of the radius of gyration also change in these configurations, reflecting their long, oblong shapes. In the examples in Table 1, we see that $I_1 > I_2$ and that $I_2 \approx I_3$ in the collapsed supercoiled arrangements, especially those at higher ΔLk where the DNA begins to change from a figure-8 shape to an interwound form. Furthermore, the writhing number increases with ΔLk beyond the critical transition from circle to figure-8, the slope dWr/dΔLk between the few reported points past the collapse being approximately 0.4 (Fig. 2a). The latter measure of configurational change in supercoiled DNA, however, can be quite misleading. According to recent finite element analysis [33] and energy minimization [34] studies, the variation of Wr with ΔLk resembles a discontinuous step function rather than a smooth linear function.

The optimized configurations obtained under the condition of 1 M salt at integral values of ΔLk are shown in Fig. 1b. As anticipated, the circular form does not persist over as wide a range of ΔLk as it does at zero salt. According to the numerical data in Tables 1 and 2 and the graphical representations in Fig. 2, the critical transition in energy from circle to figure-8, occurs somewhere in the range ΔLk = 1.5–1.75 at 1 M salt, versus ΔLk = 2.5–2.75 at zero salt. As noted above, the radius of gyration, average interphosphate distance, principal moments of the radius of gyration, and writhing number all jump suddenly at the transition point. Interestingly, the proportions of the figure-8 at the point of collapse (described in terms of R_g, I_1, I_2, I_3, and $\langle P \ldots P_{dist} \rangle$) are virtually identical to those of the corresponding figure-8 at zero salt. In other words, the effective diameter of the DNA at the circle to figure-8 transition is independent of salt concentration. Beyond the transition point, the supercoiled structures become progressively more compact as measured by the ratio of principal moments, $(I_2 - I_3)/I_1$. As at zero salt, the secondary I_2 axis becomes increasingly smaller with increase in ΔLk, while I_1 and I_3 remain practically the same. The aforementioned ratio thus approaches zero with increase of ΔLk, although more rapidly at 1 M salt than at zero salt as shown in Fig. 2b. The apparent variation of the writhing number with ΔLk beyond the circle to figure-8 collapse at 1 M salt (dWr/dΔLk = 0.3–

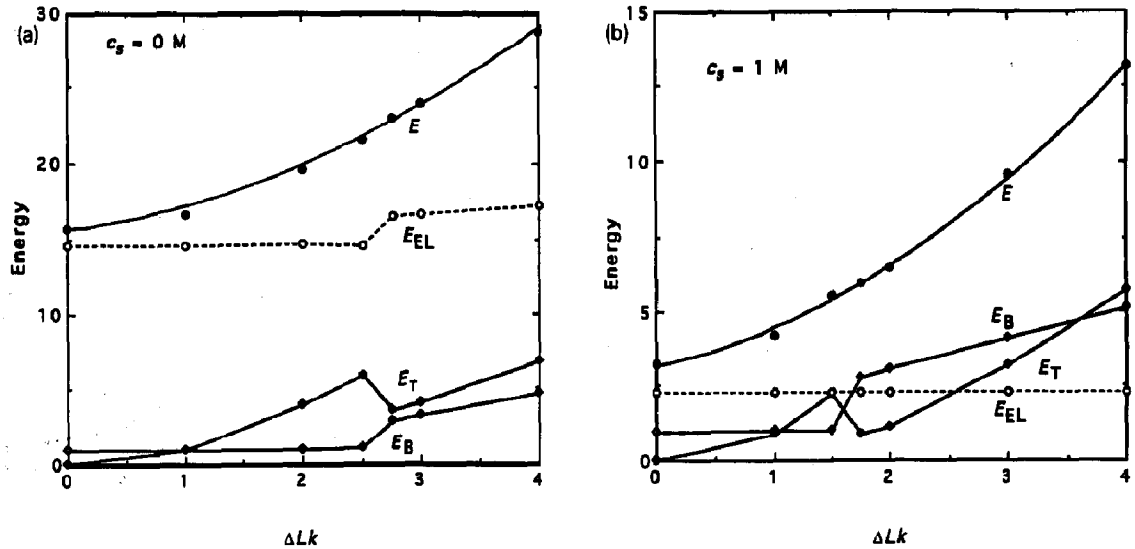

Fig. 3. Variation with ΔLk of the total reduced energy $\tilde{E}$ and its bending $\tilde{E}_B$, twisting $\tilde{E}_T$, and electrostatic $\tilde{E}_{EL}$ components for salt concentrations (a) $c_s = 0$ M (no added salt) and (b) $c_s = 1$ M. The curves passing through the total energy data are the quadratic expressions listed in the text. Note the different scales at low and high salt. See legends to Figs. 1 and 2.

0.5) is comparable to that found at zero salt, although only a few data points have been determined in either case. Small decreases in the average interphosphate distance with increase in ΔLk beyond the critical transition are apparent at both salt conditions.

As expected, the interwound structures found at 1 M salt are more compact than those at zero salt and the same value of ΔLk. The mean interphosphate distances, the radii of gyration, and ratios of moments are consistently lower and the writhing numbers consistently higher in the optimized structures at 1 M than at zero salt for supercoiled DNA with a given imposed linking number difference. The screening of phosphate charges at higher salt allows the interwound strands of the DNA to come into closer contact. At ΔLk = 3, for example, the average non-bonded contact distance between phosphates separated by more than ten nucleotides along the optimized DNA is 55.30 Å at zero salt versus 53.75 Å at 1 M salt. There are also fewer pairs of phosphate groups within 30 Å of one another at low salt than at high salt (877 versus 1458 pairs at $c_s = 0$ M and 1 M, respectively).

3.2. Optimized energy components

According to Table 2 and Fig. 3, the total energy increases smoothly with ΔLk regardless of salt concentration: The data at zero salt fall along the curve $E = 3.20 + 0.84\ \Delta Lk + 0.41\ \Delta Lk^2$, and those at 1 M salt along the curve $E = 15.44 + 0.97\ \Delta Lk + 0.60 \Delta Lk^2$. The corresponding variations of the bending, twisting, and electrostatic energy contributions, however, are more complex. As expected for the circular shape which persists at low ΔLk, the bending energy remains constant up to the critical transition point, after which it increases linearly with ΔLk (Fig. 3). Surprisingly, the increase in E_B with ΔLk is somewhat greater in the supercoiled forms at zero salt than at 1 M salt. One might expect both a slower onset of chain bending at low versus high salt (as found here) and a slower uptake of chain bending following collapse to the figure-8.

The observed variation in E at higher ΔLk is apparently driven by the twisting and electrostatic energy terms which overwhelm the bending contribution at zero salt. The bending energy exceeds the twisting energy at zero salt only when ΔLk = 0, and is as much as an order of magnitude smaller than the electrostatic energy at some non-zero values of ΔLk. In the absence of salt the electrostatic energy is dominant over all other energy contributions, and apparently dictates the final optimized structures (see Fig. 3a). At 1 M salt, in contrast, the bending energy exceeds the twisting energy over a broad range of imposed linking number differences ($0 \leqslant \Delta Lk \leqslant 1$ and $1.75 \leqslant \Delta Lk \leqslant 3.0$) (Fig. 3b). The electrostatic energy also plays a much smaller role in determining chain configuration at 1 M salt than when there is no added salt. At high salt concentrations the phosphate charges are effectively screened, and the electrostatic energy is essentially the same for circular and supercoiled DNAs. The only significant contributions to the electrostatic energy at 1 M salt come from neighboring phosphate groups which are equivalently spaced in the circular and supercoiled trajectories. At zero salt, on the other hand, E_{EL} is constant up to ΔLk = 2.5 (since all optimized structures are circles) but increases with ΔLk beyond the transition point. This is expected given both the long-range nature of the modified Debye–Hückel potential at zero salt and the smaller interphosphate distances of increasingly interwound supercoils.

The rate of change of the twisting energy with ΔLk is essentially the same at zero and 1 M salt, preceding the circle to figure-8 conversion. The variation in E_T with ΔLk, however, is greater before than after the point of collapse. The drop in E_T at the configurational transition is also not as sharp as that found in simulations of purely elastic DNA, where ΔLk at the transition point is closer in value to the writhing number of the figure-8 and the twisting energy contribution is consequently closer to zero [33,34]. The drop in E_T is, as expected, somewhat less pronounced at low than at high salt. The latter difference follows from the greater value of ΔLk, and hence the larger twist (ΔTw = ΔLk − Wr) of the figure-8 at the configurational transition under low salt conditions.

3.3. Bending to twisting ratio

Variation of the bending and twisting stiffness ratio A/C provides further information on the relative contributions of the elastic and electrostatic energy components in determining the optimized configurations of supercoiled DNA. An increase in A/C reduces the relative importance of the twisting energy, delaying the onset of supercoiling at higher ΔLk. As evident from Fig. 4 and Table 3, the 100 bp DNA model with $\Delta Lk = 3$ resists collapsing into a figure-8 under the condition of no added salt when A/C is changed from 1 to 2. The decrease in Wr found at $A/C = 2$ is not surprising given that the energy optimized $\Delta Lk = 3$ state at $A/C = 1$ is a figure-8 only slightly beyond the critical transition point. The writhing number similarly decreases with a corresponding increase of A/C at 1 M salt, although the change in overall shape and degree of overwinding is not so dramatic as in the case of no added salt. The reduction in the writhing number corresponds to an overwinding in the twist of 0.38 at high salt versus roughly one superhelical turn at zero salt.

The delay in the onset of supercoiling with increase in A/C is accompanied by an increase in total energy at both salt concentrations. At zero salt, small decreases in E_B and E_{EL} at $A/C = 2$ are compensated by a larger increase in E_T. Both bending and twisting terms are increased, while the electrostatic energy remains constant with the change in A/C at $c_s = 1$ M. The numerical values in Table 3 are reduced by a constant factor ($2\pi^2 C_0/L$, where $C_0 = 1.2755 \times 10^{-11}$ erg Å) in order to compare the relative magnitudes of individual energy terms at the two values of A/C.

3.4. Chain length dependence

The effects of chain length (at fixed $A/C = 1$) on the optimized structures in the absence and presence of salt are presented in Fig. 5 and Tables 4 and 5. Surprisingly, the increase in chain length at $\Delta Lk = 3$ leads from a figure-8 minimum at 100 bp to open circular structures at 150 and 175 bp for the case of no added salt, but to more

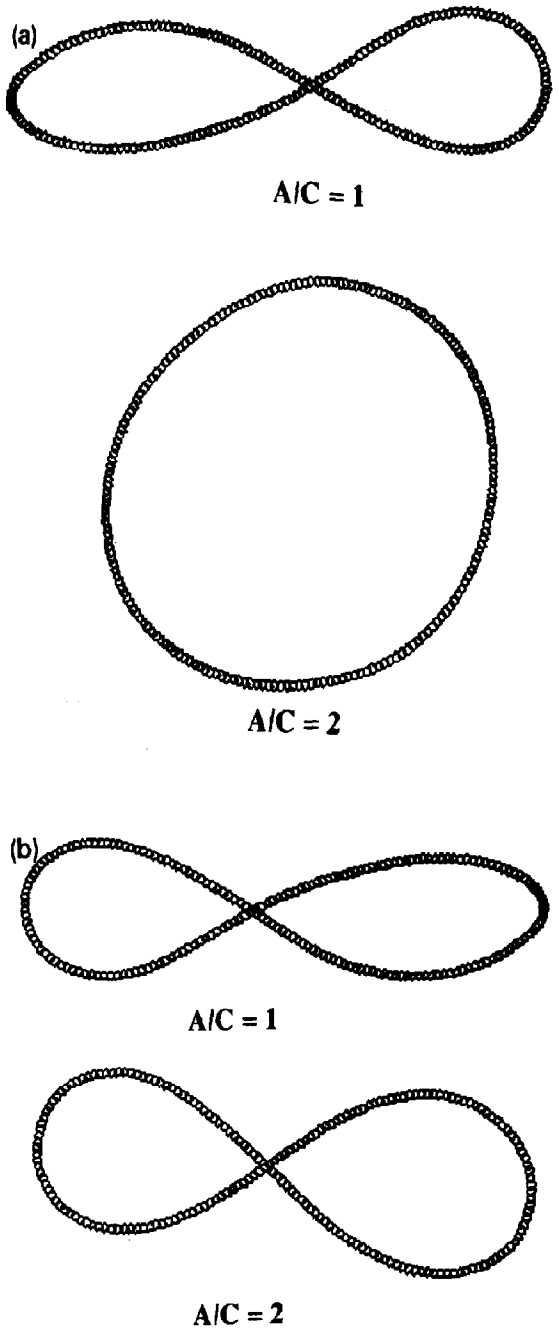

Fig. 4. Dependence of the optimized supercoiled configurations of 100-residue supercoils on the ratio A/C of the flexural rigidity coefficient to the twisting stiffness constant. The imposed linking number difference is fixed at 3. Electrostatic interactions are represented by a modified Debye–Hückel potential and excluded volume effects by a hard-sphere potential. The starting configuration is a circle of 14 evenly spaced controlling points. In (a) the salt concentration c_s is fixed at 0 M (no added salt) and in (b) $c_s = 1$ M.

Table 3
Writhing number and reduced energy components as a function of A/C and salt concentration [a]

A/C	Wr	$\tilde{E}$	$\tilde{E}_B$	$\tilde{E}_T$	$\tilde{E}_{EL}$
$c_s = 0$ M					
1.00	0.96	23.98	3.20	4.15	16.63
2.00	0.00	25.67	2.03	9.00	14.64
$c_s = 1$ M					
1.00	1.22	9.55	4.07	3.19	2.29
2.00	0.84	12.72	5.76	4.67	2.29

[a] The elastic and electrostatic model was used with $\Delta Lk = 3$ and 100 bp chain length. The energy, $\tilde{E} = E/(2\pi^2 C_0/L)$, where $C_0 = 1.2755 \times 10^{-11}$ erg Å, is a non-dimensional quantity.

highly collapsed interwound arrangements at 1 M salt. As expected from the increased number of nucleotide residues, the total energy increases with increasing chain length in both the low and the high salt regimes. The electrostatic interactions, however, play a significant role in determining the optimum spatial configuration with increase in chain length at zero salt. The increase in electrostatic energy is very pronounced since the phosphate groups are unscreened by small ions. The reduction in the twisting energy between the figure-8 ($\tilde{E}_T \approx 4$) and circle ($\tilde{E}_T \approx 9$) at $c_s = 0$ M is no longer sufficient to compensate for the corresponding increase in electrostatic repulsions between the two forms at longer chain lengths. The critical transition point is therefore shifted to larger ΔLk: thus, the observed decrease of Wr with increase of chain length at $\Delta Lk = 3$ in Table 4. It should be noted that the optimized configuration of the 175 bp chain is not a perfect circle at zero salt. The equilibrium state of this chain may not have been attained during the course of simulated annealing. The reduced bending and twisting energies of a 175 bp circle at this ΔLk ($\tilde{E}_B \approx 1$ and $\tilde{E}_T \approx 9$) generate an upper bound on $\tilde{E}$ of 60.46. (The electrostatic energy of the circle is expected be less than the value of 50.46 reported for the distorted minimum in Table 4.)

The situation is somewhat different at high salt. While the electrostatic term increases in magnitude with increase of chain length, the interplay between the bending and twisting energy continues to determine the optimum configuration when $c_s = 1$ M. The increase of the electrostatic energy with increasing chain length is much less pronounced at 1 M than zero salt. Because of its short-range nature at high salt, the modified Debye–Hückel contribution is not sensitive to the overall spatial configuration of the DNA and does not influence the onset of supercoiling. The effect of chain length on the bending energy is more complex. While the bending of individual residues is less pronounced in longer chains, the number of such terms increases. The lesser bending apparently dominates over the 100–150 bp range, leading to figure-8 structures. The computed bending energy of a Wr ≈ 1.6 chain is 5.13 for 100 bp (Table 2) versus 4.42 for 150 bp (Table 4). The data in Table 4 further suggest that the variation of E_B which accompanies interwinding of the supercoil is less sharp in longer chains. Otherwise it is difficult to account for the increase in the writhing number and the drop in E_T with chain length at high salt. The latter trends are completely opposite to those exhibited by chains with no added salt and could not be predicted ahead of time.

The chain dimensions reported in Table 5 reflect the combined effects of increasing contour length and configurational change outlined above. The radii of gyration, the largest principal moments I_1 and I_2, and the mean interphosphate distances all increase with chain length at both salt concentrations. As expected, the DNA is more expanded in the absence of salt for any given chain length. The discrepancy is greater at longer chain lengths where the low salt form opens from an interwound into a circular form. The structures at 1 M salt are more writhed (folded) but more expanded (due to larger contour length) at greater chain length.

3.5. Branched three-leaf rose versus interwound configurations

We have also carried out simulations at $\Delta Lk = 3$ using a 100 bp branched three-leaf rose as the starting structure (Fig. 6). The coordinates of this initial state are slightly deformed from those of a known stable elastic energy minimum

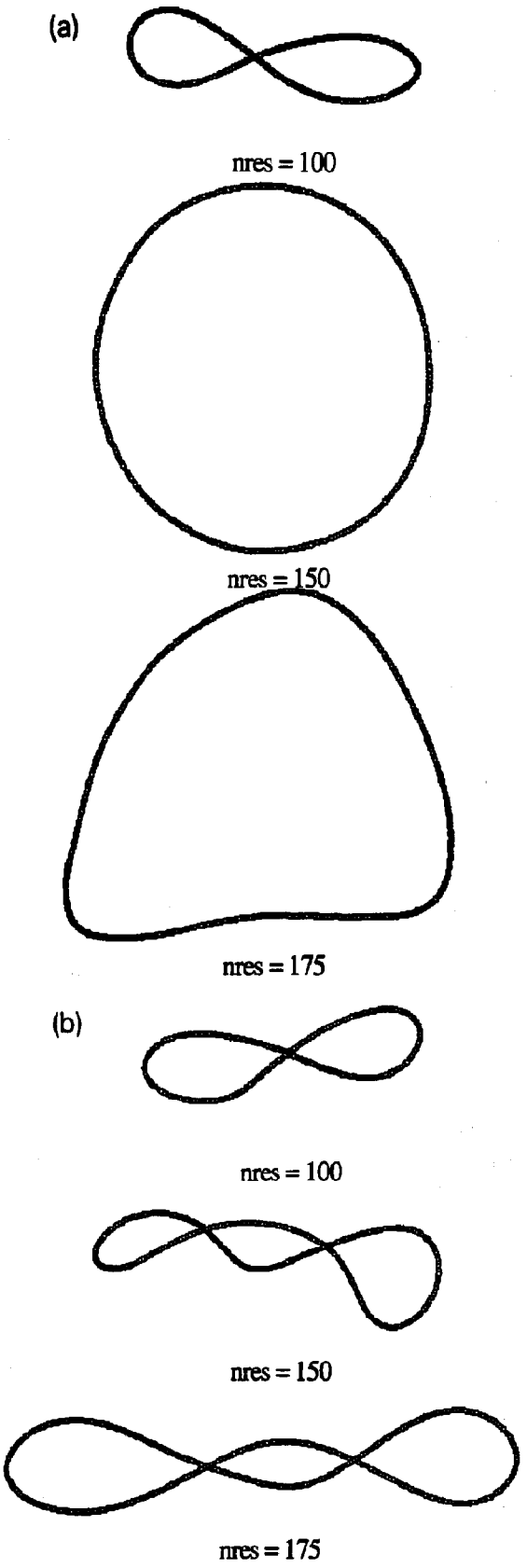

(I. Tobias, unpublished data). The branched structure is much more compact (at this particular ΔLk) than the interwound state in terms of both the mean interphosphate distance and the radius of gyration (Table 6), but is closer to a circle than an interwound supercoil in terms of the relative proportions of the principal moments of the radius of gyration ($I_1 \approx I_2 \gg I_3$). The writhing number of the three-leaf rose is comparable to that of an interwound duplex with roughly two superhelical crossings (Table 7). As a result, the variation in twisting energy upon simulated annealing is fairly small ($\Delta\tilde{E}_T = 1.26$ at $c_s = 0$ M and 0.07 at $c_s = 1$ M). The difference in energy between the branched and interwound minima lies primarily in the bending energy ($\Delta\tilde{E}_B = -3.95$ at $c_s = 0$ M and -2.95 at $c_s = 1$ M), with the electrostatic term providing some additional stabilization at zero salt ($\Delta\tilde{E}_{EL} = -1.90$). As noted above, the electrostatic term plays almost no role at high salt (the electrostatic energies of the starting branched structure and final interwound form are identical).

While the starting model in Fig. 6a can be relaxed to the apparent energy minimum, a three-lobed branched elastic energy minimum identified by deterministic methods (T. Schlick, unpublished data) is unchanged by simulated annealing. The reduced energy of the latter stable state ($\tilde{E} = 28.37$ at $c_s = 0$ M and $\tilde{E} = 10.05$ at $c_s = 1$ M) is also higher than that of the interwound global energy minimum ($\tilde{E} = 23.37$ at $c_s = 0$ M and $\tilde{E} = 8.53$ at $c_s = 1$ M).

The optimized interwound structures, shown in Fig. 6, are similar to those obtained at $\Delta Lk = 3$ with a circular starting state at 0 and 1 M salt. The energies in the present simulations, however,

Fig. 5. Examples illustrating the effect of chain length on the optimized supercoiled configurations of DNA. The imposed linking number difference is fixed at 3 and the bending to twisting ratio $A/C = 1$. The starting configuration is a circle of 14 evenly spaced controlling points. Electrostatic interactions are represented by a modified Debye–Hückel potential and excluded volume effects by a hard-sphere potential. In (a) the salt concentration c_s is fixed at 0 M (no added salt) and in (b) $c_s = 1$ M. The parameter nres is the total number of residues of the DNA.

Table 4
Writhing number and reduced energy components as a function of chain length (bp = total number of base pairs of DNA) and salt concentration [a]

bp	Wr	$\tilde{E}$	$\tilde{E}_B$	$\tilde{E}_T$	$\tilde{E}_{EL}$
$c_s = 0$ M					
100	0.96	23.98	3.20	4.15	16.63
150	0.00	45.40	1.02	8.99	35.39
175	0.09	61.11	2.20	8.45	50.46
$c_s = 1$ M					
100	1.22	9.55	4.07	3.19	2.29
150	1.61	11.50	4.42	1.93	5.15
175	1.84	13.10	4.75	1.34	7.01

[a] The elastic and electrostatic model was used with $\Delta Lk = 3$ and $A/C = 1$. The energy, $\tilde{E} = E/(2\pi^2 C/L)$, is a non-dimensional quantity.

are slightly lower than those reported above (compare Table 2 with Table 7). The writhing numbers of the optimized states are slightly higher in value and the twisting energies thus of lower magnitude at both salt concentrations. The accompanying increases in the bending energy and electrostatic term in both cases are less than the drop in E_T. The final interwound configurations are thus somewhat more compact than the corresponding minima reported above (compare the values of $\langle P \ldots P_{dist} \rangle$ in Tables 1 and 6). The effect of salt on chain geometry is thus comparable to that detailed above.

Table 5
Radius of gyration (R_g), principal moments of the radius of gyration (I_1, I_2, I_3) and the average P…P distance $\langle P \ldots P_{dist} \rangle$ as a function of chain length (bp is the total number of base pairs of DNA) and salt concentration [a]

bp	R_g (Å)	I_1 (Å)	I_2 (Å)	I_3 (Å)	$\langle P \ldots P_{dist} \rangle$ (Å)
$c_s = 0$ M					
100	44.89	42.51	13.33	5.45	55.30
150	80.59	57.73	56.21	1.69	103.56
175	88.36	65.79	58.17	9.81	113.63
$c_s = 1$ M					
100	43.89	41.98	10.72	6.99	53.75
150	66.64	64.77	13.04	8.70	80.37
175	77.39	75.45	15.93	6.50	92.67

[a] The elastic and electrostatic model was used with $A/C = 1$ and $\Delta Lk = 3$.

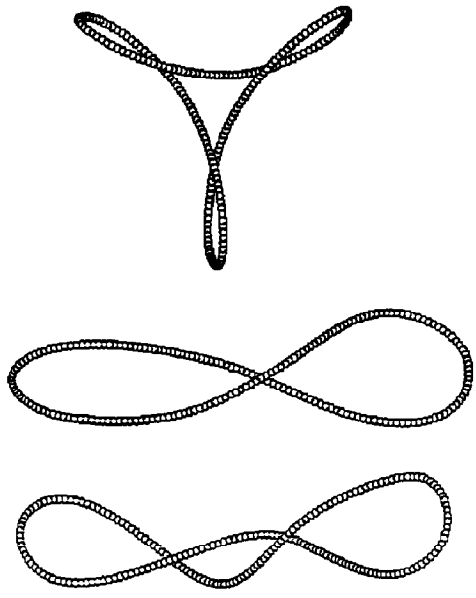

Fig. 6. Structural example illustrating the relative shape of the 100-residue branched three-leaf rose configuration with $\Delta Lk = 3$ compared to the 100-residue interwound form. The starting configuration is a symmetric three-lobed polygon with 15 controlling points (top). The optimized supercoiled configurations are shown for the cases of no added salt (middle) and 1 M salt (bottom). Electrostatic interactions are represented by a modified Debye–Hückel potential and excluded volume effects by a hard-sphere term. The bending to twisting stiffness ratio $A/C = 1$.

3.6. Electrostatic and elastic simulations versus elastic simulations

Finally, we compare our results in Table 8 with simulations of DNA supercoiling in chains of

Table 6
Radius of gyration (R_g), principal moments of the radius of gyration (I_1, I_2, I_3) and average P…P distance $\langle P \ldots P_{dist} \rangle$ for the branched three-leaf rose structure and the optimized interwound structures obtained under the condition of no added salt and 1 M salt [a]

c_s (M)	R_g (Å)	I_1 (Å)	I_2 (Å)	I_3 (Å)	$\langle P \ldots P_{dist} \rangle$ (Å)
starting three-leaf rose structure					
	31.52	21.24	21.07	9.93	40.44
optimized interwound structures					
0	44.83	43.20	9.38	7.49	54.47
1	44.13	42.83	8.89	5.87	53.22

[a] The elastic and electrostatic model was used with $A/C = 1$, $\Delta Lk = 3$, and 100 bp chain length.

Table 7
Writhing number and reduced energy components for the branched three-leaf rose structure and the optimized interwound forms obtained under the condition of no added salt and 1 M salt [a]

	Wr	$\tilde{E}$	$\tilde{E}_B$	$\tilde{E}_T$	$\tilde{E}_{EL}$
$c_s = 0$ M					
rose	1.83	28.36	7.73	1.37	19.26
interwound	1.38	23.37	3.78	2.63	17.36
$c_s = 1$ M					
rose	1.83	11.41	7.73	1.37	2.31
interwound	1.80	8.53	4.78	1.44	2.31

[a] $\tilde{E} = E/(2\pi^2 C/L)$, the energy, is a non-dimensional quantity. The elastic and electrostatic model was used with $\Delta Lk = 3$, $A/C = 1$, and 100 bp chain length.

corresponding length and ΔLk subject only to an elastic potential and a (20 Å) hard-sphere constraint. As anticipated, the optimized 100 bp DNA structures obtained in the added presence of an electrostatic energy term are more open than those found with the simple elastic model. Furthermore, the configurational differences from the elastic reference are more pronounced at 0 M than at 1 M salt. As evident from the table, the writhing number decreases at fixed ΔLk when the composite elastic/electrostatic potential is employed (more so for the case of no added salt). This trend reflects the electrostatic repulsions between phosphate groups which favor less compact structures.

According to analytical predictions based on elasticity theory [16], the critical linking number difference at which the exchange of energy between the circle and figure-8 occurs is approximately 1.4 when $A/C = 1$. As noted earlier, the phosphate repulsions included in the composite elastic/electrostatic potential energy delay the onset of the configurational transition and force the strands of the interwound form to be further apart. For $\Delta Lk = 2$ and no added salt, a circular form is found in place of a figure-8 structure when the electrostatic energy is included. At high salt ($c_s = 1$ M) the chain is collapsed, but in a slightly more open structure (Wr = 0.93) than the elastic DNA model (Wr = 0.96). In this case, the critical ΔLk is in rough agreement with the value predicted on the basis of the elastic model [16]. For $\Delta Lk = 3$, the optimized configuration is a figure-8 (with loops roughly co-planar at $c_s = 0$ M and more out-of-plane at $c_s = 1$ M and for the pure elastic model). In longer chains of 1000 bp the elastic model adopts an interwound structure [7]. Interestingly, the shortest interphosphate distances at the center of the optimized structures in Table 8 are comparable in value at zero and high salt (19.8 Å and 20.4 Å, respectively). The closest non-bonded contacts (20.3 Å) in the optimized elastic structure are also at the imposed hard-sphere limit. The length of the contact zone between long-range phosphates is, as expected, greater for the minimum energy 100 bp configuration at 1 M than 0 M salt. There are roughly 0.7 turns of distantly spaced duplex within a 21 Å separation distance and 1.9 turns within a 25 Å contact limit at 1 M salt, versus 0.5 turns of the DNA within 21 Å and 1.0 turns within 25 Å at $c_s = 0$ M. The terminal loops are thus shorter at 1 M salt than at zero salt. The loop size, as measured by long-range contact distances greater than 30 Å, is 1.9–2.4 turns of duplex at high salt versus 3.2–3.6 turns at zero salt. The loop size of the elastic model measured by this criterion is 2.3–2.7 turns of DNA. The interwound contact-zone of the elastic model is of similar dimensions to that found at 1 M salt with 1.3 turns of duplex within a 21 Å separation distance and 2.0 turns with a 25 Å limit.

Table 8
Comparison between the writhing numbers obtained with the elastic and elastic/electrostatic simulations [a]

ΔLk	Elastic model	Elastic/electrostatic model ($c_s = 1$ M)	Elastic/electrostatic model ($c_s = 0$ M)
2	0.96	0.93	0.00
3	1.31	1.22	0.96

[a] $A/C = 1$; chain length = 100 bp.

4. Summary and perspectives

The present study is a first step in understanding how the polyelectrolyte character of DNA governs the overall folding of the closed circular double helix. Until now, models of DNA super-

coiling have been based on a simple elastic treatment, where the DNA is described as an uncharged, isotropic, symmetric, and linearly elastic thin rod characterized by its local bending and twisting stiffness. The long-range repulsions of negatively charged phosphate groups have been included indirectly by increasing the magnitudes of the elastic force constants and more directly through the incorporation of Lennard-Jones or hard-sphere terms [5,7,18,35–37]. Our calculations show that specific treatment of long-range electrostatic repulsions through a modified Debye–Hückel energy term opens the DNA supercoil compared to an elastic representation of the closed circular chain. The electrostatic contribution not only influences the close contacts of interwound configurations but also shifts the critical value of the linking number difference at which the circle collapses into a figure-8 configuration. The interwound forms, for example, are more open structures than the corresponding elastic models of the same ΔLk. Moreover, the predicted opening of the chain at low salt is qualitatively consistent with the observed transition from tight to loose interwound supercoils observed upon decrease of salt concentration in cryo-electron microscopy images of highly supercoiled DNA [8,9]. The proportions of the global energy minimum state of the short DNA at the point of collapse from circle to figure-8, however, are predicted to be virtually identical at zero and 1 M salt (although occurring at different values of ΔLk).

The short (178 bp), highly supercoiled DNA minicircles visualized under the electron microscope are of chain length and superhelical density comparable to the models considered here. The topoisomers with linking number deficits of 0, −1, and −2 co-migrate in standard low salt electrophoresis buffer and exhibit near zero writhing numbers in the electron micrographs [9]. At high salt, the −2 isomer adopts a figure-8 shape under the electron microscope and moves separately from the 0 and −1 isomers on the gel. This is precisely the behavior predicted in our calculations at 1 M salt. The increased gel spacing between the −2 and −1 isomers compared to the 0 and −1 isomers is consistent with a small change in shape between the 0 and −1 states and a larger change between the −1 and −2 states (see Figs. 2 and 5). The −3 to −5 topoisomers, while not isolated and separately visualized, co-migrate with the nicked minicircle at low salt, confirming the predicted delay in the onset of writhing of supercoiled chains of 175 bp at $c_s = 0$ M in our work. The observed high salt migration of the same species is consistent with a form, such as the interwound configuration predicted for the 175 bp DNA at ΔLk = 3 and 1 M salt, that does not dramatically change in overall shape at higher imposed linking number differences.

Current limitations on computational resources prevent rigorous study of longer DNA supercoils, the comparison of different potential functions, the detailed examination of specific salt concentrations, and the analysis of large molecular ensembles. The long-range nature of the electrostatic energy necessitates detailed treatment of all pairwise phosphate–phosphate interactions. The calculations therefore cannot be enhanced by the standard use of a distance cutoff criterion. One hope for future computational speedup lies in cluster treatments, such as the fast vortex schemes commonly employed for the numerical simulation of reactive flows [38] and recently extended to studies of protein folding [39,40]. Preliminary studies show that calculations of the electrostatic energy in supercoiled DNA of 5000 bp can be enhanced by a factor of 30–50 using such algorithms [41], thereby facilitating routine studies of longer chains at naturally occurring superhelical densities. The numerical findings presented here provide an essential benchmark for what must of necessity be approximate computational treatments of longer chains.

The present data, nevertheless, reveal several interesting observations worthy of further study. One notable result is the unexpected opening of the DNA supercoil with increase in chain length at low salt concentration and the apparent collapse of the same chains at high salt. It is not clear whether this effect levels off at much longer chain lengths and whether it is sensitive to the electrostatic energy treatment. We also find that the writhing number increases with increasing salt concentration for DNA at a fixed linking

number difference over all chain lengths considered. The apparent dependence of Wr on salt concentration, however, must be tested in further simulations of longer DNAs in view of the very short length of chains treated here. Interestingly, long (2657 bp) DNA plasmids with −0.05 superhelical density show an increase in the writhing number and a tightening of interwound geometry with increasing salt concentration in cryo-electron microscopic studies [9]. The preliminary studies of branched three-leaf rose starting structures also suggest that these forms may be more energetically favorable under some conditions. The difference in bending and twisting energy between the three-leaf rose and the interwound structure of the same writhing number will be substantially reduced at longer chain lengths, so that straight and branched configurations might be of more comparable energy at high salt. Branched forms are commonly observed in electron micrographs of longer supercoiled DNA [42]. It is also of special interest to carry out additional Monte Carlo/simulated annealing simulations using the polyelectrolyte (ionic) free energy (which includes both an electrostatic and mixing energy and thereby treats the polyelectrolyte character of DNA rigorously) instead of the simple modified Debye–Hückel energy.

The effect of ionic environment on the intrinsic twist of DNA, has been studied experimentally by a number of workers [43–45]. If one is simply interested in determining the global configuration of a given topoisomer at a given salt concentration following the method described here, the results of these experiments play no role in the process. If, however, one is interested in the effect of a *changing* ionic environment on the configuration of this topoisomer, then it becomes necessary to study the experiments. For if the intrinsic twist Tw_0 changes as the salt concentration is varied, then so must ΔLk ($= Lk - Tw_0$) change. Thus, for example, if, as some of the work suggests, DNA winds more tightly with increasing salt concentration, then the corresponding increase in the value of Tw_0 would be accompanied by a decrease in ΔLk. One can then use the theory being presented here to determine the changed shape of the plasmid, taking into account not only the new salt concentration, but also the new value of ΔLk.

Acknowledgement

The authors are grateful to Professor Paul Hagerman for helpful discussions and to Mr. Andrew Olson for structure analysis. This work was supported by the U.S. Public Health Service under grants GM34809 and GM36284. Calculations were performed at the Rutgers Center for Computational Chemistry, the Pittsburgh Supercomputer Center, and the National Cancer Institute Supercomputing Facility. MOF was the recipient of a John von Neumann Fellowship from Rutgers University.

References

[1] W.R. Bauer, F.H.C. Crick and J.H. White, Sci. Am. 243 (1980) 118.
[2] L.F. Liu and J.C. Wang, Proc. Natl. Acad. Sci. USA 84 (1987) 7024.
[3] W.R. Bauer, Ann. Rev. Biophys. Bioeng. 7 (1978) 287.
[4] J.H. White, Am. J. Math. 91 (1969) 693.
[5] W.K. Olson and P. Zhang in: Molecular design and modeling: concepts and applications, Part B. Antibodies and antigens, nucleic acids, polysaccharides, and drugs, ed. J.J. Langone (Academic Press, New York, 1991) p. 403.
[6] M.-H. Hao, Ph.D. Thesis, Rutgers University, New Brunswick (1988).
[7] M.-H. Hao and W.K. Olson, Macromolecules 22 (1989) 3292.
[8] M. Adrian, B. ten Heggeler-Bordier, W. Wahli, A.Z. Stasiak, A. Stasiak and J. Dubochet, EMBO J. 9 (1990) 4451.
[9] J. Bednar, P. Furrer, A. Stasiak, J. Dubochet, E.H. Egelman and A.D. Bates, J. Mol. Biol. 235 (1994) 825.
[10] C.J. Benham, Proc. Natl. Acad. Sci. USA 74 (1977) 2397.
[11] C.J. Benham, Biopolymers 18 (1979) 609.
[12] C.J. Benham, Phys. Rev. A 39 (1989) 2582.
[13] F.B. Fuller, Proc. Natl. Acad. Sci. USA 68 (1971) 815.
[14] M. Le Bret, Biopolymers 18 (1979) 1709.
[15] M. Le Bret, Biopolymers 19 (1980) 619.
[16] M. Le Bret, Biopolymers 23 (1984) 1835.
[17] P. Zhang, W.K. Olson and I. Tobias, Comp. Polymer Sci. 1 (1991) 3.
[18] T. Schlick and W.K. Olson, J. Mol. Biol. 223 (1992) 1089.
[19] T. Schlick and W.K. Olson, Science 257 (1992) 1110.

[20] M.E. Mortenson, Geometric Modeling (Wiley, New York, 1985).
[21] R. Chandrasekaran and S. Arnott in: Landolt-Börnstein numerical data and functional relationships in science and technology, Group VII/1b. Nucleic acids, ed. W. Saenger, (Springer, Berlin, 1989) p. 31.
[22] G.S. Manning, Quart. Rev. Biophys. (1978) 179.
[23] P.J. Flory, Statistical mechanics of chain molecules (Wiley–Interscience, New York, 1969).
[24] L.D. Landau and E.M. Lifshitz, Course of theoretical physics, Vol. 5, Statistical physics (Pergamon Press, Oxford, 1980).
[25] G.S. Manning, Biopolymers 20 (1981) 1751.
[26] J. Wilcoxon and J.M. Schurr, Biopolymers 22 (1983) 2273.
[27] G.S. Manning, Biopolymers 27 (1988) 1529.
[28] F. Tanaka and H. Takahashi, J. Chem. Phys. 83 (1985) 6017.
[29] J.H. White, in: Mathematical methods for DNA sequences, ed. M.S. Waterman (CRC Press, Boca Raton, 1989) p. 225.
[30] F.B. Fuller, Proc. Natl. Acad. Sci. USA 75 (1978) 3557.
[31] N. Metropolis, A.W. Rosenbluth, M.N. Rosenbluth, A. Teller and E. Teller, J. Chem. Phys. 21 (1953) 1087.
[32] S. Kirkpatrick, C.D. Gelatt and M.P. Vecchi, Science 220 (1983) 671.
[33] Y. Yang, I. Tobias and W.K. Olson, J. Chem. Phys. 98 (1993) 1673.
[34] T. Schlick, W.K. Olson, T. Westcott and J.P. Greenberg, Biopolymers (1994), in press.
[35] K.V. Klenin, A.V. Vologodskii, V.V. Anshelevich, A.M. Dykhne and M.D. Frank-Kamenetskii, J. Mol. Biol. 217 (1991) 413.
[36] A.V. Vologodskii, S.D. Levene, K.V. Klenin, M.D. Frank-Kamenetskii and N.R. Cozzarelli, J. Mol. Biol. 227 (1992) 1224.
[37] V.V. Rybenkov, N.R. Cozzarelli and A.V. Vologodskii, Proc. Natl. Acad. Sci. USA 90 (1993) 5307.
[38] K. Chua, T.R. Quackenbush and A. Leonard, Report C.D.I. 92-03, Continuum Dynamics, Inc., Princeton, NJ (1992).
[39] R.H. Stote, D.J. States and M. Karplus, J. Chim. Phys. 88 (1991) 2419.
[40] A. Warshel, J. Chem. Phys. 97 (1992) 3100.
[41] M.O. Fenley, K. Chua and W.K. Olson (1993), in preparation.
[42] C.D. Boles, J.H. White and N.R. Cozzarelli, J. Mol. Biol. 213 (1990) 931.
[43] C.F. Anderson and W. Bauer, Biochemistry 17 (1978) 594.
[44] D.M. Hinton and V. Bode C., J. Biol. Chem. 250 (1975) 1071.
[45] W.H. Taylor and P.J. Hagerman, J. Mol. Biol. 212 (1990) 363.